MATHEMATICAL BIOSCIENCES
AND ENGINEERING
Volume **12**, Number **6**, December **2015**

doi:10.3934/mbe.2015.12.1277

pp. **1277–1288**

ONCOGENE-TUMOR SUPPRESSOR GENE FEEDBACK INTERACTIONS AND THEIR CONTROL

Baltazar D. Aguda*

DiseasePathways LLC, Bethesda, Maryland, 20814, USA

Ricardo C.H. del Rosario

Computational and Systems Biology, Genome Institute of Singapore
60 Biopolis St., #02-01 Genome, 138672, Singapore

Michael W.Y. Chan

Department of Life Science & Institute of Molecular Biology
National Chung Cheng University, Min-Hsiung, China-Yi, Taiwan

Abstract. We propose the hypothesis that for a particular type of cancer there exists a key pair of oncogene (OCG) and tumor suppressor gene (TSG) that is normally involved in strong stabilizing negative feedback loops (nFBLs) of molecular interactions, and it is these interactions that are sufficiently perturbed during cancer development. These nFBLs are thought to regulate oncogenic positive feedback loops (pFBLs) that are often required for the normal cellular functions of oncogenes. Examples given in this paper are the pairs of MYC and p53, KRAS and INK4A, and E2F1 and miR-17-92. We propose dynamical models of the aforementioned OCG-TSG interactions and derive stability conditions of the steady states in terms of strengths of cycles in the qualitative interaction network. Although these conditions are restricted to predictions of local stability, their simple linear expressions in terms of competing nFBLs and pFBLs make them intuitive and practical guides for experimentalists aiming to discover drug targets and stabilize cancer networks.

1. **Introduction.** Genes involved in driving cancers are broadly categorized as oncogenes (tumor-promoting) and tumor suppressor genes. To transform cells, many known oncogenes (OCGs) require an activating mutation in only one of their alleles (gain-of-function mutation) while tumor suppressor genes (TSGs) require deactivating mutations in both alleles (loss-of-function mutations). Besides genetic mutations, cancer can also arise from epigenetic perturbations such as amplified gene expression due to multiple copies of OCGs (with normal DNA sequence) in chromosomes, and overexpression due to covalent modifications and subsequent hyperactivation of gene promoters.

A comprehensive census of human cancer genes has been carried out [13, 27, 15] and attempts are being made to link these genes in interaction networks and molecular pathways [16]. A key question being addressed is the identity of the set of 'driver' genes that initiate or maintain the progression of a given type of cancer [30, 17]. We list in Table 1 a few of the OCGs and TSGs that are currently

2010 *Mathematics Subject Classification.* Primary: 92B05, 92C42; Secondary: 34C23.

Key words and phrases. Oncogene-tumor suppressor gene pairs, myc, p53, kras, ink4a, e2f1, miR-17-92, network stability, feedback loops, cycle strength, drug targets.

* To whom correspondence should be addressed.

considered as driver genes for various human cancers, and we provide a few examples of OCG-TSG interactions from this list.

We propose the following hypotheses and analyze representative models to generate predictions: (I) In a normal cell, there exists a pair of driver genes composed of an OCG and a TSG that are involved in a strong negative feedback loop of interactions to maintain system stability, and (II) To drive cancer, certain perturbations destabilize the OCG-TSG interactions and permit the OCG to overwhelm the TSG.

We give a brief review in Section 2 of the literature that supports our proposal that the normal OCG-TSG network is composed of an OCG positive feedback loop (pFBL) and an OCG-TSG negative feedback loop (nFBL). In Section 3, we show that we can make general conclusions on network stability based only on the qualitative information contained in the OCG-TSG network topology and signs of interactions. We then analyze in Section 4 an ODE (ordinary differential equations) model of the assumed normal OCG-TSG network to identify its stable regions in parameter space and what perturbations can lead to escape from these regions. In Section 5, we analyze a network of interactions between the oncogene MYC and the tumor suppressor gene TP53 (usually referred to as p53); this important network has been proposed to coordinate the cellular and cancer-relevant processes of proliferation and differentiation [4]. Finally, we give our conclusions and suggest practical applications of our results in Section 6.

2. **Examples of OCG-TSG feedback interactions.**

Prior to their respective cancer-driving activating and deactivating perturbations, OCGs and TSGs are essential elements in a normal cellular response to environmental and internal stimuli. For example, increased expression of the oncogene MYC and activation of its corresponding protein product (myc) are observed upon growth-factor stimulation of a cell, followed by increased expression of myc-target genes that drive DNA replication and of the tumor suppressor gene p53 [29]. We have reviewed in a previous paper [4] the indirect and direct pathways by which myc activates p53, as well as pathways through which p53 inhibits myc activity. Thus, we can interpret the increase in p53 activity as a negative feedback to increase in myc activity. Other examples of negative feedback loops (nFBLs) between OCG-TSG pairs are shown in Fig. 1. Details of the nFBL between MYC or E2F1 and miR-17-92 (microRNA) are reviewed in [5], and details of the nFBL between KRAS and INK4A are discussed in [2].

Many oncogenic pFBLs have been reported [21, 28, 12, 10, 24, 23, 5]. The oncogenic pFBLs involving MYC and E2F1 are well documented [21, 28, 5]. The pFBLs involving KRAS (specifically, kras-GTP, the active GTP-bound form of protein kras) and its effectors, as well as pFBLs involving kras microRNAs, have been reviewed [2]. These pFBLs are predicted to be required for setting thresholds of activation and generating switch-like behavior of the protein products of OCGs [2].

3. **Stability analysis of OCG-TSG qualitative networks using cycles.**

Using only qualitative information from the topology and signs of the interactions between the OCG and TSG, we can derive general local stability properties of the system. For convenience of matrix representation later, let X_1 and X_2 represent the OCG and TSG activities, respectively. First-order decay kinetics for both species is assumed. Besides the perturbations of the parameters and variables of a system,

TABLE 1. List of potential driver oncogenes and tumor suppressor genes in some human cancers. Genes in *italics* are listed among the high-confidence mutational driver cancer genes proposed by Tamborero *et al.* [30].

Cancer Type	**Oncogenes**	**Tumor Suppressor Genes**	**Refs.**
Lung	*KRAS, EGFR, BRAF*, PI3KCA, *ERBB2, CCND1*, MET, MYC, MDM2, CDK4, CCNE1	*TP53, PTEN, STK11*, *RB1, KEAP1, CDKN2A*, *NF1*, FHIT, DAPK1, RASSF1A, *APC*, RARB, *CDH1*	[9], [18], [8], [30]
Breast	*ERBB2*, PI3KCA, MYC, *CCND1*	*RB1, BRCA1, BRCA2*, *TP53, PTEN, ATM*, CHK2, *RUNX1*, RUNX2, RUNX3	[19]
Colorectal	*KRAS, BRAF*, PI3KCA	*APC, TP53,* TGFBRII, *CTNNB1*, SMAD4	[26]
Ovarian	RAB25, EVI1, EIF5A2, PRKC1, PI3KCA, FGF1, MYC, *EGFR,* NOTCH3, *KRAS, ERBB2, PIK3R1*, CCNE1, AKT2, AURKA	ARHI, RASSF1A, DLEC1, DAB2, PLAGL1, *BRCA1*, *BRCA2,* WWOX, *TP53*, *PTEN*	[27]
Gastric	*ERBB2, KRAS,* COX-2, MET, TERT	RUNX3, *TP53, APC*, DCC, MLH1, TGFBRII, BAX, IGFIIR, *CDH1*	[31]
Head & Neck	MMP7, MMP9, MMP3, *EGFR, CCND1*	*TP53, CDKN2A,* DCC, *PTEN,* RASSF1A, DAPK, *CDH1*	[14], [25], [22]
Glioblastoma	MYC, *EGFR*, CDK6, MDM2, *KRAS*	*TP53, PTEN, NF1* *CDKN2A, RB1*	[1], [7]

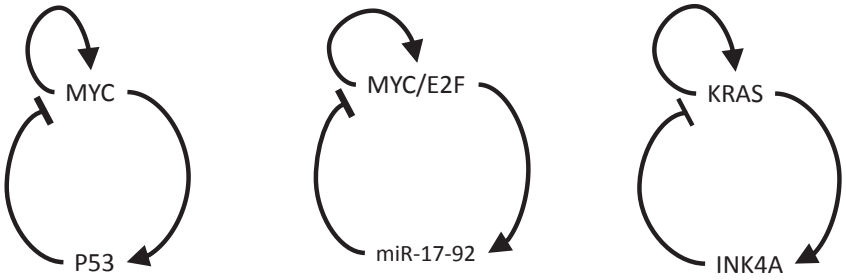

FIGURE 1. Examples of OCG-TSG network involving an OCG positive feedback loop and an OCG-TSG negative feedback loop. Arrows mean 'activation' ($m_{ij} > 0$), and hammerheads mean 'inhibition' ($m_{ij} < 0$). See text for the meaning of m_{ij}. A 2-cycle is a positive (negative) feedback loop if $m_{ij}m_{ji} > 0$ ($m_{ij}m_{ji} < 0$). A 1-cycle is a positive (negative) feedback loop if $m_{ii} > 0$ ($m_{ii} < 0$).

creation of new interactions is another perturbation that must be taken into account (deletion of an interaction is carried out by setting associated parameters to zero). Thus, a pathway from the OCG that inhibits the TSG (in parallel to the assumed normal pathway that activates the TSG) is included in the model below to account for cases where perturbations (*e.g.*, gene mutations) create such interactions (see [4] for examples). This inhibitory pathway from the OCG to the TSG will be represented separately in the model equations to monitor the effect of such perturbations. We assume that the dynamics of the system can be described by the following ODEs:

$$\frac{dX_1}{dt} = f_1(X_1, X_2) - \delta_1 X_1 \tag{1}$$

$$\frac{dX_2}{dt} = f_{2p}(X_1) + f_{2n}(X_1) - \delta_2 X_2 \tag{2}$$

subject to the following constraints:

$$\frac{\partial f_1}{\partial X_1} > 0, \frac{\partial f_1}{\partial X_2} < 0, \frac{\partial f_{2p}}{\partial X_1} > 0 \text{ , and } \frac{\partial f_{2n}}{\partial X_1} < 0. \tag{3}$$

The first constraint represents the self-activation or positive 1-cycle of X_1 corresponding to the oncogenic pFBLs mentioned in the preceding section. It is assumed that the inhibition of the OCG by the TSG acts against the pFBL of the OCG - this is represented by the second constraint above. No pFBL involving the TSG is considered as they have not been documented as often as OCGs. The elements of the linearized (Jacobian) matrix, evaluated at some steady states of X_1 and X_2, are

$$m_{11} = \frac{\partial(dX_1/dt)}{\partial X_1} = m_{11p} + m_{11n} \text{ where } m_{11p} = \frac{\partial f_1}{\partial X_1} > 0, m_{11n} = -\delta_1 < 0 \tag{4}$$

$$m_{12} = \frac{\partial(dX_1/dt)}{\partial X_2} = \frac{\partial f_1}{\partial X_2} < 0 \tag{5}$$

$$m_{21} = \frac{\partial(dX_2/dt)}{\partial X_1} = m_{21p} + m_{21n} \text{ where } m_{21p} = \frac{\partial f_{2p}}{\partial X_1} > 0, m_{21n} = \frac{\partial f_{2n}}{\partial X_1} < 0 \tag{6}$$

$$m_{22} = \frac{\partial(dX_2/dt)}{\partial X_2} = -\delta_2 < 0. \tag{7}$$

We draw a qualitative network (qNET) diagram based on the signs of the m_{ij}'s using the convention: X_j activates X_i if $m_{ij} > 0$, and X_j inhibits X_i if $m_{ij} < 0$. The qNET diagram corresponding to the linearization of Eqns. (1)-(2) is shown in Fig. 2.

The characteristic polynomial whose roots are the eigenvalues (λ) of the Jacobian matrix (evaluated at steady states) is written as follows

$$P_2(\lambda) = \lambda^2 + \alpha_1 \lambda + \alpha_2 = 0 \tag{8}$$

where the coefficients α_i's can be expressed in terms of the elements m_{ij} of the Jacobian matrix:

$$\alpha_1 = -m_{11} - m_{22} \text{ and } \alpha_2 = -m_{12}m_{21} + m_{11}m_{22}. \tag{9}$$

We use the intuitive language of cycle strengths to express our stability analysis. The 1-cycle involving species X_i has the strength $S_i = m_{ii}$, and the 2-cycle between

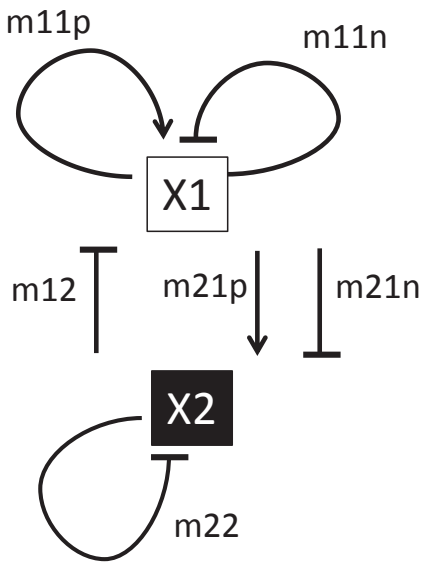

FIGURE 2. The qNET diagram based on the elements of the Jacobian matrix of Eqns. (1)-(2). See also Eqns. (4)-(7). Arrows mean 'activation', and hammerheads mean 'inhibition'.

species X_i and X_j has the strength $D_{ij} = m_{ij}m_{ji}$. Thus, the coefficients of $P_2(\lambda)$ can be expressed in terms of cycle strengths:

$$\alpha_1 = -(S_{1p} + S_{1n}) - S_2 \text{ where } S_{1p} = m_{11p} \text{ and } S_{1n} = m_{11n} \tag{10}$$

$$\alpha_2 = -D_{12} + S_1 S_2 = -(D_p + D_n) + (S_{1p} + S_{1n})S_2 \tag{11}$$

$$\text{where } D_p = m_{21n}m_{12} \text{ and } D_n = m_{21p}m_{12}.$$

For the general n-th order $P_n(\lambda)$, the coefficients in terms of cycle strengths are given in [3]. Analysis of the roots of $P_2(\lambda)$ gives the following results:

(i) The system's steady state is stable if $\alpha_1 > 0$ and $\alpha_2 > 0$; these conditions correspond, respectively, to

$$(S_{1p} + S_{1n}) < -S_2 \text{ and } (D_p + D_n) < S_2(S_{1p} + S_{1n}) \tag{12}$$

(ii) There exists only one positive real eigenvalue if $\alpha_2 < 0$, regardless of the sign of α_1. This condition corresponds to

$$(D_p + D_n) > S_2(S_{1p} + S_{1n}) \tag{13}$$

(iii) The two eigenvalues have positive real parts if $\alpha_1 < 0$ and $\alpha_2 > 0$. These conditions correspond, respectively, to

$$(S_{1p} + S_{1n}) > -S_2 \text{ and } (D_p + D_n) < S_2(S_{1p} + S_{1n}) \tag{14}$$

(iv) Saddle-node bifurcation occurs when

$$(D_p + D_n) = S_2(S_{1p} + S_{1n}) \tag{15}$$

(v) Hopf bifurcation occurs when

$$(S_{1p} + S_{1n}) = -S_2 \text{ and } (D_p + D_n) < S_2(S_{1p} + S_{1n}) \tag{16}$$

The phase diagram showing stability regions is given in Fig. 3.

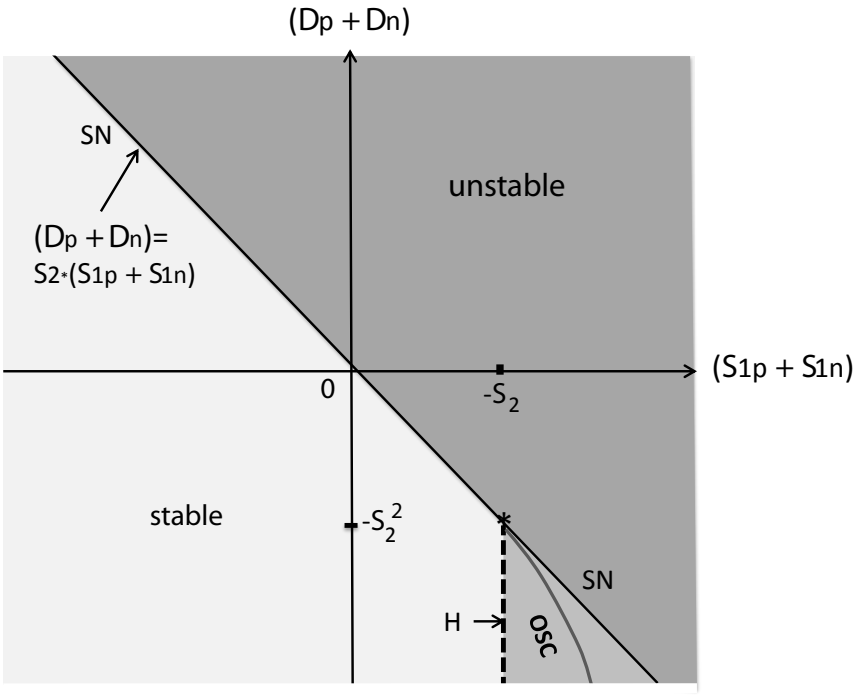

FIGURE 3. Phase diagram based on the Jacobian matrix of Eqns. (1)-(2). The saddle-node (SN) and Hopf (H) bifurcation lines are indicated. Regions with unstable steady states are shaded grey (including the region to the right of H). The oscillatory region (OSC) is bounded by H and the grey parabolic curve defined by $\alpha_2 = \alpha_1^2/4$.

4. **Bifurcation analysis of the E2F1-(miR-17-92) network.** A model we analyzed earlier [5] involves the oncogene E2F1 and the tumor suppressor miR-17-92 (see Fig. 1b). We consider this model here to illustrate the results in the preceding section. The model dynamics is described by the following ODEs:

$$\frac{dX_1}{dt} = \alpha + \left(\frac{k_1 X_1^2}{\gamma_1 + X_1^2 + \gamma_2 X_2}\right) - \delta_1 X_1 \tag{17}$$

$$\frac{dX_2}{dt} = \beta + k_2 X_1 - \delta_2 X_2 \tag{18}$$

where the parameters $k_1, k_2, \alpha, \beta, \gamma_1, \gamma_2, \delta_1$ and δ_2 are all non-negative. This model's phase diagram only covers the region below the abscissa in Fig. 3 where $(D_p+D_n) < 0$, since $D_p = 0$ (no positive 2-cycle) and $D_n < 0$. With the same bifurcation parameters used in [5] (namely, α' and γ_2' – the dimensionless versions of α and γ_2, respectively), Li *et al.* [20] constructed a phase diagram showing regions of monostability, bistability and oscillations; and in Fig. 4, we reconstructed this phase diagram using a slightly different set of parameters and showing a wider picture. Parameter α' corresponds to a constitutive rate of expression of E2F1 (the rate being assumed proportional to growth factor concentration) and γ_2' corresponds to a coefficient of inhibition of E2F1 by miR-17-92.

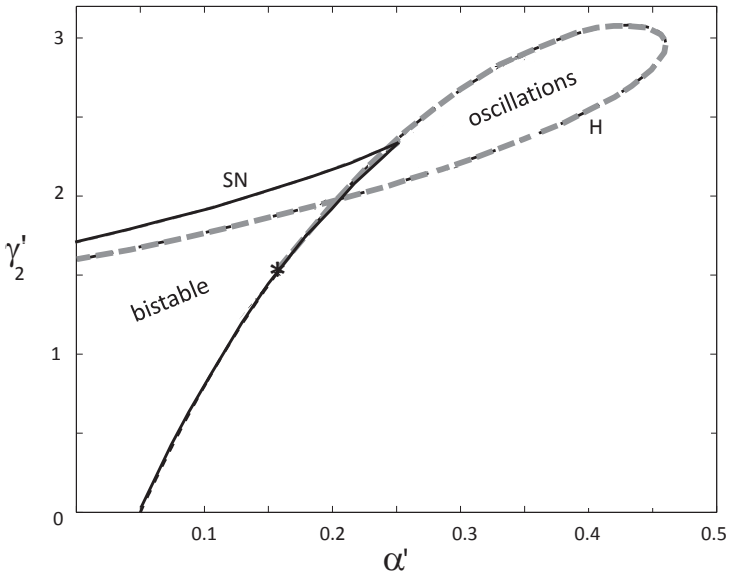

FIGURE 4. Phase diagram of the E2F1-(miR-17-92) model. The coordinates are dimensionless parameters corresponding to α and γ_2 in Eqns. (17)-(18). See Ref. [5] for the dimensionless equations. $\alpha' = (k_2/(\delta_1\beta))\alpha, \gamma_2' = (k_2^2/(\beta\delta_2))\gamma_2, \gamma_1' = (k_2^2/\beta^2)\gamma_1, \varepsilon = \delta_2/\delta_1, \kappa = k_1k_2/(\delta_1\beta)$.Parameters: $\varepsilon = 0.1, \kappa = 5, \gamma_1' = 1$. Software used is the MATCONT package [11] in MATLAB (The MathWorks, Inc., Natick, Massachusetts, USA).

For this model, the non-zero steady-state cycle strenghts are

$$S_{1p} = \frac{2k_1X_1(\gamma_1 + \gamma_2X_2)}{(\gamma_1 + X_1^2 + \gamma_2X_2)^2} \tag{19}$$

$$S_{1n} = -\delta_1 \tag{20}$$

$$S_2 = -\delta_2 \tag{21}$$

$$D_n = -\frac{k_1k_2\gamma_2X_1^2}{(\gamma_1 + X_1^2 + \gamma_2X_2)^2} \tag{22}$$

where X_1 and X_2 are evaluated at steady state. There is a nonlinear mapping of the steady-state manifold $X_1(\alpha', \gamma_2')$ associated with Fig. 4 to the plane in Fig. 3; this mapping is sketched in Fig. 5.

One can see from Eqns. (19)-(22) that only the negative 1-cycles, S_{1n} and S_2, possess parameters that uniquely control them – namely, δ_1 and δ_2, respectively. As shown in Fig. 3, increasing the magnitude of S_2 (*i.e.*, increasing δ_2 – the decay rate constant of the TSG) will push the left boundary of the oscillatory region towards the right of Fig. 3, effectively increasing the area of stability. The magnitude of the slope of the saddle-node (SN) line in Fig. 3 increases too, thereby decreasing further the oscillatory region. Similarly, increasing the magnitude of S_{1n} by increasing the decay rate constant δ_1 of X_1 leads to decreasing $(S_{1p} + S_{1n})$, thereby pushing the system to the left of Fig. 3 – *i.e.*, towards more stability. Thus, the negative 1-cycles S_{1p} and S_{1n} are stabilizing.

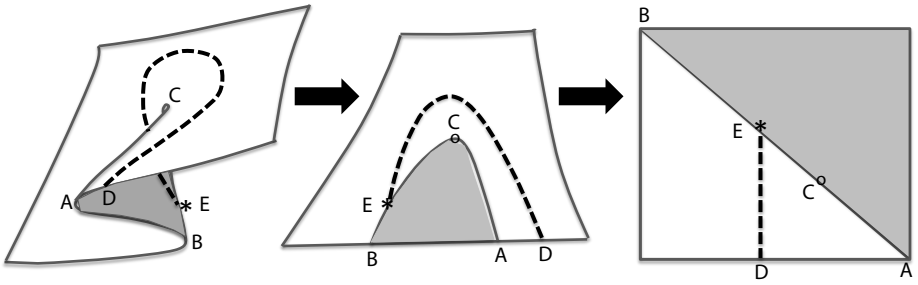

FIGURE 5. A sketch of the mapping from the 2-dimensional steady-state manifold, $X_1(\alpha', \gamma_2')$, of the E2F1-(miR-17-92) model (corresponding to Fig. 4) to the plane in Fig. 3. First step is to unfold the surface to give the picture in the middle. Second, turn it over and stretch to form. Points on the resulting plane can be mapped one-to-one to points on the plane of Fig. 3.

Although Fig. 3 provides a simple and intuitive picture of analyzing stability in terms of competing cycles, it has a disadvantage in that it loses information on parameters that give multiple steady states. For instance, there could be three different points (two points in the stable region and one point in the unstable region) in Fig. 3 that correspond to the same set of parameters. Furthermore, there is the important question of whether one can associate cancer initiation with a switch to a higher steady state of the oncogene due to network instability. We have addressed this question in our earlier paper [5] where we propose that it is the magnitude of the increase in OCG activity that determines whether it enters a 'cancer zone' where the probability of cancer-promoting downstream events is high (see [5] for a discussion on the cancer zone postulate). Nevertheless, the results of our cycle analysis summarized in Fig. 3 have the advantage of easily identifying destabilizing cycles.

5. **An OCG-TSG network that coordinates cell proliferation and differentiation.** The transcription factors myc and p53 drive cell proliferation and differentiation in antagonistic ways. In an earlier work [4], we reviewed pathways by which myc drives both the cell cycle and apoptosis, and by which myc inhibits cell differentiation; and pathways by which p53 inhibits the cell cycle, drives apoptosis, and promotes cell differentiation [4]. As depicted in Fig. 1a, myc and p53 interact in a negative feedback loop. In some cancers (*e.g.*, glioblastoma), genetic mutations and certain epigenetic perturbations create pathways that effectively permit myc to inhibit p53 (also reviewed in [4]). We proposed that this myc-p53 network is a core control mechanism in coordinating cell proliferation and differentiation, and have carried out a qualitative kinetic modeling of the system. Our first model [4] ignored the pFBL involving myc. Here, we re-analyze the myc-p53 network using a slightly modified set of equations that includes the pFBL of myc as well as terms for constitutive expressions of myc and p53. The ODEs are listed below where m = activity of myc and p = activity of p53.

$$\frac{dm}{dt} = \alpha + \frac{k_1 m^2}{\gamma_1 + m^2 + \gamma_2 p} - \delta_1 m \tag{23}$$

$$\frac{dp}{dt} = \beta + k_2 m + \frac{k_4}{k_3 + m} - \delta_2 p. \tag{24}$$

The steady state strengths of the 1-cycles (S_{1p}, S_{1n}, S_2) and the 2-cycles (D_p, D_n), evaluated at the steady states of m and p, are

$$S_{1n} = -\delta_1 \tag{25}$$

$$S_2 = -\delta_2 \tag{26}$$

$$S_{1p} = \frac{2k_1 m(\gamma_1 + \gamma_2 p)}{(\gamma_1 + m^2 + \gamma_2 p)^2} \tag{27}$$

$$D_n = -\frac{k_1 k_2 \gamma_2 m^2}{(\gamma_1 + m^2 + \gamma_2 p)^2} = -\frac{k_2 \gamma_2 m}{2(\gamma_1 + \gamma_2 p)} S_{1p} \tag{28}$$

$$\begin{aligned} D_p &= \frac{k_1 k_4 \gamma_2 m^2}{(k_3 + m)^2(\gamma_1 + m^2 + \gamma_2 p)^2} = -\frac{k_4}{k_2(k_3 + m)^2} D_n \\ &= \frac{k_4 \gamma_2 m}{2(k_3 + m)^2(\gamma_1 + \gamma_2 p)} S_{1p}. \end{aligned} \tag{29}$$

Except for S_{1n} and S_2, all the other cycle strengths depend on all parameters (the steady states m and p are functions of all parameters). Thus, except for S_{1n} and S_2, it is difficult to manipulate the cycles independently from the others; and it is cumbersome and non-intuitive to use the exact stability conditions that involve finding the steady states of m and p from Eqns. (23)-(24) followed by using Eqns. (25)-(29) in the inequality of (12). In the following, we list two sufficient conditions for stability that are easier to implement experimentally than the exact conditions of (12).

(i) The stable region defined by $(D_p + D_n) < 0$ and $(S_{1p} + S_{1n}) < 0$ (see Fig. 3) correspond, respectively, to

$$k_2 > \frac{k_4}{(k_3 + m)^2} \tag{30}$$

$$\delta_1 > \frac{2k_1 m(\gamma_1 + \gamma_2 p)}{(\gamma_1 + m^2 + \gamma_2 p)^2} \tag{31}$$

These conditions correspond to the dominance of the negative cycles D_n and S_{1n} over the positive cycles S_p and S_{1p}, respectively. In practice, one would experiment on progressively increasing the rate coefficients k_2 and δ_1 to find the thresholds predicted by (30)-(31). Increasing k_2 and δ_1 will also tend to increase the tumor suppressor activity p and decrease the oncogene activity m, respectively.

(ii) The stable region defined by $(D_p + D_n) < -S_2^2$ and $(S_{1p} + S_{1n}) < -S_2$ (see Fig. 3) correspond, respectively, to:

$$k_2 > \frac{k_4}{(k_3 + m)^2} + \frac{\delta_2^2(\gamma_1 + m^2 + \gamma_2 p)^2}{k_1 \gamma_2 m^2} \tag{32}$$

$$\delta_1 + \delta_2 > \frac{2k_1 m(\gamma_1 + \gamma_2 p)}{(\gamma_1 + m^2 + \gamma_2 p)^2} \tag{33}$$

Condition (32) imposes a higher threshold for k_2 than in (30), but (33) is a weaker condition than (31) because in (33) one has the freedom to choose which of δ_1 or δ_2 , or both, to manipulate. As in (i), increasing k_2 and δ_1 will tend to increase p and decrease m, respectively. Note, however, that increasing δ_2 decreases p (the TSG) and could lead to a stable steady state with high m contrary to the goal of suppressing the OCG.

Another strategy to increase the probability of satisfying conditions (30)-(33) would be to lower the thresholds for k_2 and δ_1 or δ_2 by decreasing the strengths of the positive cycles, namely, D_p (by decreasing k_4) and S_{1p} (by decreasing k_1).

6. **Conclusions.** We propose that two feedback loops in the interactions between an OCG and a TSG are key targets in the initiation of cancer: one is a pFBL involving the OCG which endows it the ability to amplify proliferative signals and to set a threshold for activation, and the other is a nFBL between the OCG and TSG – specifically, the OCG promoting the activity of the TSG and the latter inhibiting the former. Using only this qualitative information, we have derived simple general conditions in terms of the strengths of cycles for the steady states of the OCG and TSG to be stable. We also have shown that transitions to instability are governed by saddle-node and Hopf bifurcations – the former characterized by switching between separated branches of steady states, and the latter by oscillatory behavior. As illustrated by the MYC-p53 couple, perturbations may include the introduction of a new pathway – in this case, the OCG inhibiting the TSG – which creates a pFBL (double inhibition) between the OCG and the TSG. The pFBLs of the network are destabilizing while the nFBLs are stabilizing, and we have derived conditions that can be used to manipulate the relative strengths of these cycles to control stability. The strengths of the negative 1-cycles depend on unique parameters (corresponding to the individual decay rate coefficients of the OCG and TSG, assuming first-order kinetics) and are therefore easy to control, and predictions on the existence of threshold values for these cycle strengths to maintain stability are given. In contrast, the strengths of the 2-cycles are more difficult to control by varying one parameter at a time (but it could be done after solving the steady states of the OCG and TSG as functions of parameters, and substituting these steady states and parameters to the expressions of the 2-cycle strengths). Ultimately, the advantage of stability analysis using the language of cycles is that it can identify specific destabilizing cycles that can be targeted and suppressed to return the network to stability. Identifying the dominant destabilizing cycles could be a useful strategy for finding drug targets (perturbation targets) because identification of a small number of destabilizing cycles reduces the complexity of the network control problem.

REFERENCES

[1] B. D. Aguda, Network pharmacology of glioblastoma, *Curr Drug Discov Technol.*, **10** (2013), 125–138.

[2] B. D. Aguda, The significance of the feedback loops between KRas and Ink4a in pancreatic cancer, in *Molecular Diagnostics and Therapy of Pancreatic Cancer* (ed. A. Azmi), Elsevier Academic Press, (2014), 281–296.

[3] B. D. Aguda and A. B. Goryachev, From pathways databases to network models of switching behavior, *PLoS Comput Biol.*, **3** (2007), 1674–1678.

[4] B. D. Aguda, Y. Kim, H. S. Kim, A. Friedman and H. A. Fine, Qualitative network modeling of the Myc-p53 control system of cell proliferation and differentiation, *Biophys J.*, **101** (2011), 2082–2091.

[5] B. D. Aguda, Y. Kim, M. G. Piper-Hunter, A. Friedman and C. B. Marsh, MicroRNA regulation of a cancer network: Consequences of the feedback loops involving miR-17-92, E2F and Myc, *Proc Natl Acad Sci USA*, **105** (2008), 19678–19683.

[6] R. C. Bast, B. Henessy and G. B. Mills, Jr., The biology of ovarian cancer: New opportunities for translation, *Nat Rev Cancer*, **9** (2009), 415–428.

[7] Cancer Genome Atlas Research Network, Comprehensive genomic characterization defines human glioblastoma genes and core pathways, *Nature*, **494** (2013), p506.

[8] Cancer Genome Atlas Research Network, Comprehensive molecular profiling of lung adenocarcinoma, *Nature*, **511** (2014), 543–550.

[9] W. A. Cooper, D. C. Lam, S. A. O'Toole and J. D. Minna, Molecular biology of lung cancer, *J Thorac Dis.*, **5** (2013), S479–S490.

[10] J. Daniluk, Y. Liu, D. Deng, J. Chu, H. Huang, S. Gaiser, Z. Cruz-Monserrate, H. Wang, B. Ji and C. D. Logsdon, An NF-κB pathway-mediated positive feedback loop amplifies Ras activity to pathological levels in mice, *J Clin Invest.*, **122** (2012), 1519–1528.

[11] A. Dhooge, W. Govaerts and Y. A. Kuznetsov, MATCONT: A Matlab package for numerical bifurcation analysis of ODEs, *ACM Trans Math Softw (TOMS)*, **29** (2003), 141–164.

[12] J. Drost and R. Agami, Transformation locked in a loop, *Cell*, **139** (2009), 654–656.

[13] P. A. Futreal, L. Coin, M. Marshall, T. Down, T. Hubbard, R. Wooster, N. Rahman and M. R. Stratton, A census of human cancer genes, *Nat Rev Cancer*, **4** (2004), 177–183.

[14] P. K. Ha, S. S. Chang, C. A. Glazer, J. A. Califano and D. Sidransky, Molecular techniques and genetic alterations in head and neck cancer, *Oral Oncol*, **45** (2009), 335–339.

[15] `http://cancer.sanger.ac.uk/cancergenome/projects/census/`.

[16] `http://ncg.kcl.ac.uk` (network of cancer genes).

[17] C. Kandoth, M. D. McLellan, F. Vandin, K. Ye, B. Niu, C. Lu, M. Xie, Q. Zhang, J. F. McMichael, M. A. Wyczalkowski, M. D. Leiserson, C. A. Miller, J. S. Welch, M. J. Walter, M. C. Wendl, T. J. Ley, R. K. Wilson, B. J. Raphael and L. Ding, Mutational landscape and significance across 12 major cancer types, *Nature*, **502** (2013), 333–339.

[18] J. E. Larsen and J. D. Minna, Molecular biology of lung cancer: Clinical applications, *Clin Chest Med.*, **32** (2011), 703–740.

[19] E. Y. Lee and W. J. Muller, Oncogenes and tumor suppressor genes, *Cold Spring Harb Perpect Biol.*, **2** (2010), a003236.

[20] Y. Li, Y. Li, H. Zhang and Y. Chen, MicroRNA-mediated positive feedback loop and optimized bistable switch in a cancer network involving miR-17-92, *PLoS One*, **6** (2011), e26302.

[21] P. Liao, W. Wang, M. Shen, W. Pan, K. Zhang, R. Wang, T. Chen, Y. Chen, H. Chen and P. Wang, A positive feedback loop between EBP2 and c-Myc regulates rDNA transcription, cell proliferation, and tumorigenesis, *Cell Death Dis.*, **5** (2014), e1032.

[22] L. Mao, W. K. Hong and V. A. Papadimitrakopoulou, Focus on head and neck cancer, *Cancer Cell*, **5** (2004), 311–316.

[23] G. M. Marshall, P. Y. Liu, S. Gherardi, C. J. Scarlett, A. Bedalov, N. Xu, N. Iraci, E. Valli, D. Ling, W. Thomas, M. van Bekkum, E. Sekyere, K. Jankowski, T. Trahair, K. L. Mackenzie, M. Haber, M. D. Norris, A. V. Biankin, G. Perini and T. Liu, SIRT1 promotes N-Myc oncogenesis through a positive feedback loop involving the effects of MKP3 and ERK on N-Myc protein stability, *PLoS Genet.*, **7** (2011), e1002135.

[24] K. Nowak, K. Kerl, D. Fehr, C. Kramps, C. Gessner, K. Killmer, B. Samans, B. Berwanger, H. Christiansen and W. Lutz, BMI1 is a target gene of E2F-1 and is strongly expressed in primary neuroblastomas, *Nucleic Acids Res.*, **34** (2006), 1745–1754.

[25] B. Perez-Ordoñez, M. Beauchemin and R. C. Jordan, Molecular biology of squamous cell carcinoma of the head and neck, *J Clin Pathol.*, **59** (2006), 445–4453.

[26] C. C. Pritchard and W. M. Grady, Colorectal cancer molecular biology moves into clinical practice, *Gut.*, **60** (2011), 116–129.

[27] T. Santarius, J. Shipley, D. Brewer, M. R. Stratton and C. S. Cooper, A census of amplified and overexpressed human cancer genes, *Nat Rev Cancer*, **10** (2010), 59–64.

[28] K. Tago, M. Funakoshi-Tago, H. Itoh, Y. Furukawa, J. Kikuchi, T. Kato, K. Suzuki and K. Yanagisawa, Arf tumor suppressor disrupts the oncogenic positive feedback loop including c-Myc and DDX5, *Oncogene*, **34** (2015), 314–322.

[29] P. Takahashi, A. Polson and D. Reisman, Elevated transcription of the p53 gene in early S-phase leads to a rapid DNA-damage response during S-phase of the cell cycle, *Apoptosis*, **16** (2011), 950–958.

[30] D. Tamborero, A. Gonzalez-Perez, C. Perez-Llamas, J. Deu-Pons, C. Kandoth, J. Reimand, M. S. Lawrence, G. Getz, G. D. Bader, L. Ding and N. Lopez-Bigas, Comprehensive identification of mutational cancer driver genes across 12 tumor types, *Sci Rep.*, **3** (2013), p2650.

[31] M. Vauhkonen, H. Vauhkonen and P. Sipponen, Pathology and molecular biology of gastric cancer, *Best Pract Res Clin Gastroenterol*, **20** (2006), 651–674.

Received September 22, 2014; Accepted March 20, 2015.

E-mail address: bdaguda@gmail.com
E-mail address: rcdelros@gmail.com
E-mail address: chanmwy@gmail.com